Lattice-matched Four-Junction Tandem Solar Cell Including Two Dilute Nitride Bottom Junctions

Arto Aho, Riku Isoaho, Lauri Hytönen, Timo Aho, Marianna Raappana, Ville Polojärvi, Antti Tukiainen, Jarno Reuna, Severi Mäkelä, Mircea Guina

Corresponding author: arto.j.aho@tut.fi, Optoelectronics Research Centre, Tampere University of Technology, Tampere, Finland

Abstract

Monolithic four-junction solar cells incorporating two dilute nitride (GaInNAsSb) bottom junctions are reported. The dilute nitride junctions have bandgaps of 0.9 eV and 1.2 eV, while the top junctions have bandgaps of 1.4 eV and 1.9 eV. By using experimental based parametrization, it was estimated that the four junction solar cell could theoretically exhibit efficiency levels of 34.7% at one sun, 43.2% at 100 suns, and 46.4% at 1000 suns for AM1.5D illumination. The most challenging sub-cell in terms of fabrication is the GaInNAsSb bottom junction with 0.9 eV bandgap. For this sub-cell, a background doping level down to $5{\cdot}10^{14}$ cm^{-3} and a high charge carrier lifetime up to 2–4 ns is reported, which reflects high values for current and voltage. An experimental AlGaAs/GaAs/GaInNAsSb/GaInNAsSb solar cell structure was fabricated by molecular beam epitaxy. At one sun AM1.5D illumination the experimental cell exhibited an efficiency of 25%, an average quantum efficiency of 91% and an open circuit voltage, which is about 87% of the estimated potential. The cell exhibited maximum efficiency of 37% at 100 suns concentration.

1. Introduction

Four-junction (4J) solar cells can theoretically exhibit efficiency levels of over 50% [1]. Yet to date, the best 4J cells exhibit a maximum efficiency of 46% under concentrated sunlight. Such devices are fabricated either by wafer bonding solar cells made on GaAs and InP substrates [2], or by using an inverted metamorphic architecture [3; 4]. Generally speaking, these fabrication methods require extensive and nonstandard processing techniques, such as release of the epitaxial structure needed for the inverted architecture, handling of two different substrates in the case of bonded cells, and introduction of supporting structure for the finished cell. In addition, in the case of metamorphic structures, the possible residual strain complicates the processing due to self-rolling of the film and the need for thick metamorphic buffer layers increases the material utilization. Ultimately, these nonstandard processes result in increased costs, processing time and process related sensitivity, and have negative effect on the yield and indeed the throughput.

In an industrially and economically favorable fabrication scenario, the four junction solar cells would be manufactured using established fabrication steps utilized for standard triple junction cells, such as lattice-matched GaInP/Ga(In)As/Ge and GaInP/GaAs/GaInNAsSb, or upright metamorphic GaInP/GaInAs/Ge. Lattice-matched approach in particular is interesting since thick buffer layers between the junctions are not needed, and mature tunnel junctions developed for the standard triple junction cells can be directly utilized. In addition, due to strain balance, the solar cell processing for lattice-matched solar cells is straightforward and easy to implement even for thin wafers or membranes.

In principle, lattice-matched multijunction solar cell (MJSC) on GaAs or Ge substrates can be fabricated using junctions based on standard III–V semiconductors and lattice-matched GaInNAsSb. For the integration, the standard III-V materials can cover bandgap range from 2.0 eV to 1.4 eV and similarly GaInNAsSb compounds

can be tuned to efficiently harvest the photon energy range from 1.4 eV to 0.8 eV. By using ideal bandgaps for the sub-junctions, conversion efficiencies beyond 50% can be achieved for MJSC with 5 to 6 junctions. The bottleneck for the lattice-matched approach has been the challenge to develop and integrate high performance dilute nitride sub-cells in a MJSC stack. Typical GaInNAsSb-based solar cells have exhibited poor current and voltage caused by high back ground doping levels (> 10^{16} cm^{-3}) and short charge carrier lifetimes (<< 1 ns). These challenges have been recently alleviated by using molecular beam epitaxy (MBE). Using this technique high performance triple junction cells with 44% conversion efficiency under concentrated sunlight [5] as well as 31% conversion efficiency for one sun space illumination [6] have been demonstrated. On the other hand, only little progress for the development of 4J dilute nitride solar cells has been reported, with initial demonstrations employing Ge as bottom-junction and only one dilute nitride sub-cell [7-9].

In our study, we take a different approach and focus on a tandem architecture shown in Figure 1, which exploits the potential of dilute nitrides also for realizing the bottom-junction with a bandgap down to 0.9 eV. This kind of multijunction approach aims for maximal V_{oc}, and at least in concentrated photovoltaic (CPV) applications, a high voltage design is preferred to reduce ohmic losses. Yet, maybe the most important benefit is the fact that the entire structure is fully based on III-V compounds without any concerns of unintentional intermixing of group IV elements and III-V materials. In addition, for the cost reduction, the approach is compatible with substrate recycling processes, which have been demonstrated for different GaAs-based solar cells [10-12].

Here, we report on the theoretical performance and the progress made for the fully lattice-matched 4J cell on GaAs substrates. We use GaInP or AlGaAs, GaAs and two GaInNAsSb junctions with bandgaps of 1.9 eV, 1.4 eV, 1.2 eV and 0.9 eV, respectively. For the experimental proof of concept in this paper, we used AlGaAs as the top junction. The cell performance is projected for different conditions, and we also discuss potential improvements for the structure and future prospects for the approach.

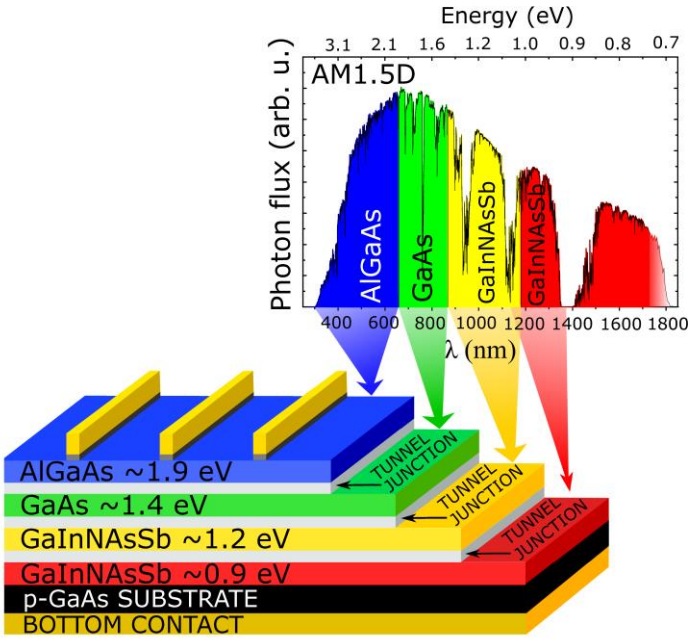

Figure 1. *Schematic structure of 4J cell with 1.9 eV, 1.4 eV, 1.2 eV and 0.9 eV junctions. The 1.2 eV and 0.9 eV junctions are based on GaInNAsSb.*

2. Theoretical efficiency limits for the 4J solar cell

For the theoretical performance estimation of the 4J solar cell, we used 1D multijunction diode modelling that includes the effect of series resistance in the circuit but excludes shunt resistive components, which can be neglected for high-quality devices [13]. For the model, an ideality factor of 1.5 was assumed for all the sub-cells. We used bandgap open circuit voltage offsets of 0.4 V for the top cells and 0.5 V for the bottom cells similarly as in earlier study for multijunction cells [13]. The assumption for the ideality factor is based on the comparing modeled and experimental operation for MBE-grown III/V solar cell materials. The model estimate may not be valid for all possible designs, solar cell sizes, and III-V solar cell materials. For this paper, the approximation was validated for an MBE-grown GaInP/GaAs/GaInNAsSb triple junction cell with bandgaps of 1.9 eV, 1.4 eV and 0.97 eV; the fit between experimental data and model for this case is revealed in Figure 5. The same assumptions were also verified for dilute nitride triple junction space solar cells [6]. The bandgap voltage offset values used have been achieved experimentally for thick single junction cells biased with one-sun illumination, full spectrum excitation, and without optical filters placed on top of the cell, and were reported, for example, in references [14] and [13].

The theoretical current-matching short-circuit current densities (J_{sc}) and the estimated maximum efficiencies for ASTM G173-03 AM0 and ASTM G173-03 AM1.5D spectra illumination are summarized in Table 1. The table 1 includes two 4J designs corresponding to bottom junction bandgaps of either 0.95 eV or 0.90 eV. In addition, we have used average external quantum efficiency (EQE) values of 100%, 95% and 90% for the entire 4J operation band. This average EQE value is calculated for the sum (total) of the four EQE curves of the 4J. Since the cells are in series, also the generation currents of the four sub-cell need to match.

Table 1. *Current-matching J_{sc} values for the 4J cell with 0.95 or 0.90 eV bandgap bottom cell.*

	J_{sc} (mA/cm^2) for AM0 (G173-03 ETR)		J_{sc} (mA/cm^2) for AM1.5D (1000 W/m^2)		One sun efficiency (%): AM0		One sun efficiency (%): AM1.5D	
Bottom cell E_g (eV)	*0.95*	*0.90*	*0.95*	*0.90*	*0.95*	*0.90*	*0.95*	*0.90*
EQE_{av} = 100%	*15.67*	16.47	*12.88*	13.16	*33.0*	34.2	*36.5*	36.6
EQE_{av} = 95%	*14.89*	15.64	*12.24*	**12.51**	*31.3*	32.4	*34.6*	34.7
EQE_{av} = 90%	*14.11*	14.82	***11.60***	**11.85**	*29.5*	30.6	*32.7*	32.8

The average EQE limits are based on physical limitation set by the spectrum, antireflection coating (ARC), and grid shadowing. A high performance MJSC with a nearly unity average internal quantum efficiency (IQE) accompanied with an ARC with average reflection of 2% and finger grid pattern with shadowing of only 3% could achieve up to 95% average EQE. On the other hand, several multijunction cells worldwide have been reported to exhibit 90% average EQE values and therefore this value has been selected for the lower limit [13]. For current matching with this bandgap combination, the two top most junctions need to be thinned. The exact thickness depends on the material dependent absorption coefficients. Examples for the top cell thinning strategy and more discussion on the topic has been addressed for example by A. P. Kirk [15].

For the experiments in this paper, we used thickness of 600 nm for both of the top cells. The total thickness for the top cells is therefore 1.2 μm, which is significantly less than approximately 4 μm for the optimal current generation and power output for 2J solar cell with the bandgaps of 1.9 eV and 1.4 eV.

Depending on the average EQE and bottom junction bandgap, the simulated efficiencies with one sun AM1.5D illumination is in range from 32.7% to 36.6%. For one sun AM0 excitation, the corresponding efficiency span is from 29.5% to 34.2%. Based on the simulations, it seems that it is beneficial to push the bottom cell bandgap down to 0.9 eV instead of using bandgap of 0.95 eV. An example of simulated I-V characteristics at AM1.5D one sun illumination is presented in Figure 2a.

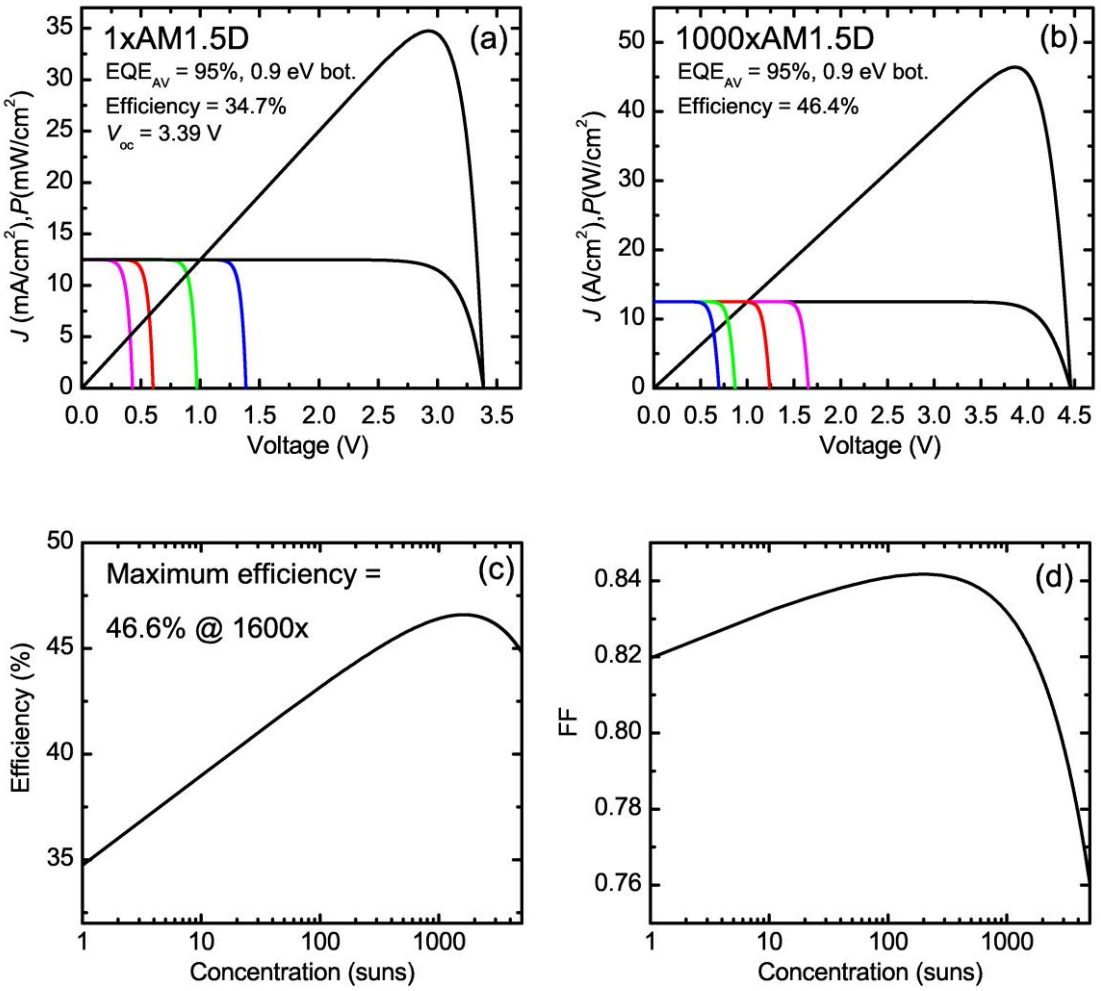

Figure 2. *(a) One sun I-V curve simulation results for the 4J cell and (b) 1000 suns I-V curve simulation results for the 4J cell. (c) 4J cell efficiency simulation and (d) fill factor (FF) at different concentrations.*

CPV applications are currently the most relevant terrestrial applications for III-V MJSC structures. Selected CPV estimated characteristics are presented in Figures 2b-2d. In the simulations we assume that the cell has 8 mΩ·cm^2 series resistance, which has been estimated from the experimental results fitted for a GaInP/GaAs/GaInNAsSb dilute nitride 3J cell with a 3% grid coverage measured at 1000 suns. At 1000 suns AM1.5D illumination, the 4J cell has efficiency of 46.4%, as shown in Figure 2b. With the given simulation parameters, the maximum efficiency of 46.6% is achieved at 1600 suns concentration. In addition, the cell efficiency within its operation band for photon energies higher than 0.9 eV, i.e., intra-band efficiency, is 52.7% at 1000 suns. If photons that are transparent to the junctions, i.e. photons with energies lower than 0.9 eV, could be dumped, the heat generation could be decreased by up to 22%. This is practically helpful option for maintaining high efficiencies in real world applications even at 1600 suns.

3. Experiments

The experimental 4J solar cell structure was grown on p-GaAs substrates with a Veeco Gen20 MBE system equipped with solid sources for Al, Ga, In, As, P and Sb, and a radio frequency (RF) plasma source for the incorporation of activated N. Detailed studies on the growth dynamics, which include for example the control of N incorporation with RF plasma sources, are reported elsewhere [16-18]. The solar cells structures were processed using photolithography and mesa etching in devices with an area of 1 mm ×1 mm. Subsequent to

the processing, the cells were mounted on a copper heatsink and top contacts were wire bonded to a separate contact pad. For characterization we used quantum efficiency (QE), reflectance, and light biased current-voltage (LIV) measurements at one sun and 100 suns AM1.5D. The QE system was calibrated by known Si and Ge detectors. For the MJSC measurements, the sub-cells which were not under investigation were light biased to over-generate compared to the sub-cell which was studied [19]. We used LEDs with different emission wavelengths for the top cells, and a narrow linewidth 1.2 μm emission wavelength dilute nitride laser diode for the biasing of the bottom cell [20]. For the LIV measurements, the cells were evaluated at one sun with an in-house built multiband solar simulator and at high concentrations with a commercial steady-state CPV solar simulator (TriSol system from OAI corporation). In addition, the one sun measurements were conducted also with the TriSol system for verification. The simulators were calibrated using known solar cells with different bandgaps ranging from 1.9 eV to 0.7 eV. For the bottom cell material quality analysis we also used PC1D simulation tool for the simulation of the bottom cell EQE characteristics.

4. Experimental results and discussion

The I-V characteristics of two 4J experimental cells are presented in Figure 3a. The best cell with TiO_x/SiO_x ARC measured at one sun AM1.5D (1000 W/m^2) exhibit a conversion efficiency of 25%, with J_{sc} of 11.7 mA/cm^2 and V_{oc} of 2.94 V. These values have not yet reached the simulated performance level for the 4J but still resulted in a high average EQE of 91% and a measured-simulated V_{oc} ratio of 87% (2.94 V/3.39 V). Partly, the lower V_{oc} values originate from the fact that we used a small area component with perimeter recombination affecting the cell V_{oc}. Based on the literature and calculations, 1 mm ×1 mm component could suffer up to 0.1 V decrease in the V_{oc} when compared to a 5 mm × 5 mm cell [21]. For comparison, modelled IV characteristics for the 4J are also presented in the Figure 3a, this estimate is based on the results measured for separate experimental component cells of the 4J. The comparison in Figure 3a reveal 0.1 V penalty for V_{oc}, which is indeed expected due to the complexity of the integration and due to the early stage of the of the development.

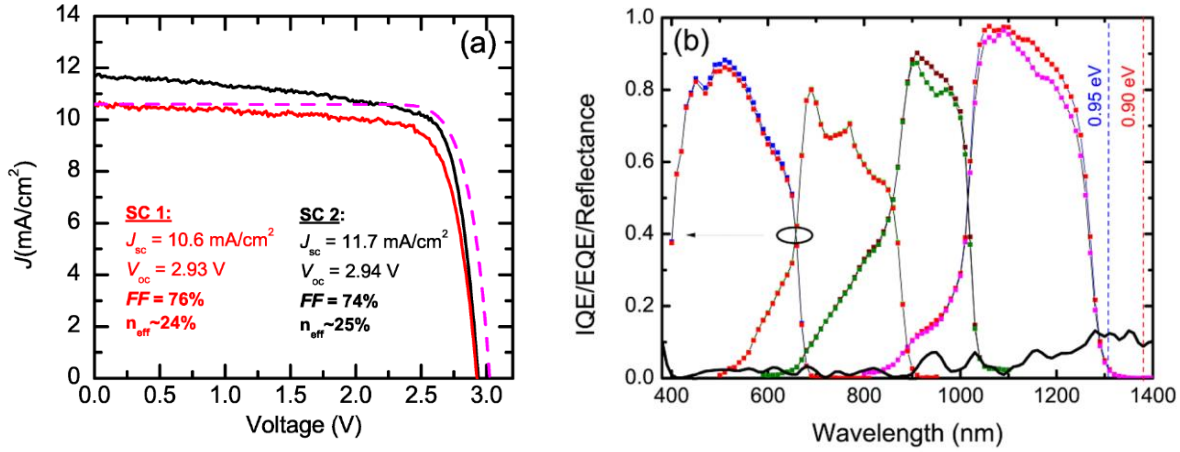

Figure 3. *(a) One sun measurement of two experimental 4J (SC1, SC2) with two dilute nitride bottom cells and modelled IV-characteristics. The modelling is based on experimental results measured at one sun for component cells, for which V_{oc} values of 2.2 V for the top pair, 0.52 V for the 3rd junction and 0.30 V for the 4th junction were measured. (b) IQE, EQE and reflectivity measurement of the 4J cell. The QE of the bottom junctions are measured from the 4J and the QE of the two top junctions are measured separately from the cell comprising only the top junctions. The cells were measured at 25°C.*

The IQE performance for the 4J cell is presented in Figure 3b. The data reveals the absorption edges of the sub-junctions. For the bottom junction, the absorption tail extends down to energies below 0.95 eV. Up to

1100 nm, the sum of the IQE values for the dilute nitride bottom junctions is nearly unity. Also for the top cells, the performance is excellent, but the absorption of high energy photons in the top most tunnel junction and the non-ideal short wavelength collection efficiency for the top cell hinders the average IQE of the device. Losses can be seen for example at the IQE cross point for the top cells where the total IQE is only 80%. It is obvious that highly transparent top tunnel junction would give additional advance for the cell performance as increased current generation. It has been observed that minimizing the amount of GaAs in the top tunnel junction has resulted in excellent transparency [22]. We estimate that the light absorption in the topmost TJ consisting of 30 nm of GaAs could reduce the GaAs sub-junction current by 0.6 mA/cm^2. If we would thin the TJ down to 10 nm, the estimated loss could be only 0.2 mA/cm^2. For the EQE performance of the device, the ARC coating deposited on top of the cell also reduces the current generation of the bottom and top cells.

For a highly efficient 4J cell ARC needs to be carefully balanced to achieve the highest performance. We use a dielectric double layer TiO_x/SiO_x coating deposited on top of the 4J cell. For this type of ARC, the efficient antireflection band is extending from 400 nm to 1300 nm (see Figure 3b). Photons at wavelengths outside this spectral range will be significantly reflected and this part of energy will be lost. For CPV applications, the photon harvesting below 400 nm wavelength require implementations that might not be economically feasible, at least for terrestrial AM1.5D applications. Therefore, reduced performance for a solar cell for the spectral range below 400 nm is not necessary the most critical issue at the system level. When comparing to a MJSC with Ge bottom cell, the situation is significantly different. For Ge based cells, the spectral band is much wider and is extended up to ~1700 nm. Therefore, a simple and efficient ARC for a 4J cell with Ge bottom junction exhibiting high current generation is significantly more demanding to make than for the 4J cell with higher bandgaps studied in this work.

Table 2. *Calculated J_{sc} values from EQE/IQE and multiband measurements, and the difference between the J_{sc} values for AM1.5D.*

	J_{sc} (mA/cm^2) for AM0		J_{sc} (mA/cm^2) for AM1.5D (1000 W/m2)			
Junction	IQE	EQE	IQE	EQE	Multiband	J_{sc}(EQE) - J_{sc}(Multiband)
1st (Top)	14.5	14.70	11.74	11.52	**11.8** (Top 2J)	-0.28 (-2%)
2nd	12.4	12.38	11.17	11.13	**11.8** (Top 2J)	-0.67 (-6%)
3rd	11.9	11.56	10.1	9.9	**10.6** (Full 4J)	-0.70 (-7%)
4th	13.2	12.54	11.3	10.8	**10.6** (Full 4J)	+0.20 (+2%)

Based on the EQE and the reflectance measurements of the ARC, the bottom cell loses about 0.5 mA/cm^2 and the top junction loses about 0.2 mA/cm^2 when compared to the IQE values summarized in Table 2. Based on EQE, we estimate that the bottom junction (with corresponding J_{sc} = 10.8 mA/cm^2) or the third junction (with corresponding J_{sc} = 9.9 mA/cm^2) limit the cell current. The J_{sc} values measured with the OAI solar simulator at one sun conditions (shown in Figure 3a) were 10.6 mA/cm^2 (SC 1) and 11.7 mA/cm^2 (SC 2). We want to note here that the J_{sc} calculated for the third cell is affected by the biasing conditions of the QE measurements, which explains partly the misfit between the I-V data. According to the results for a triple junction cell incorporating the three topmost cells (not shown here), the J_{sc} value for the 3rd cell is over 11 mA/cm^2. The measurement of the 3rd cell turned out to be challenging due to lack of proper bias lights for the measurement of MJSC structure. For bottom cell biasing we used a 1.2 μm dilute nitride laser. Then LEDs were used for exciting the top cells under 600 nm. However, the GaAs junction cannot be efficiently biased because its EQE is less than 20% for the wavelengths below 600 nm (see Figure 3).

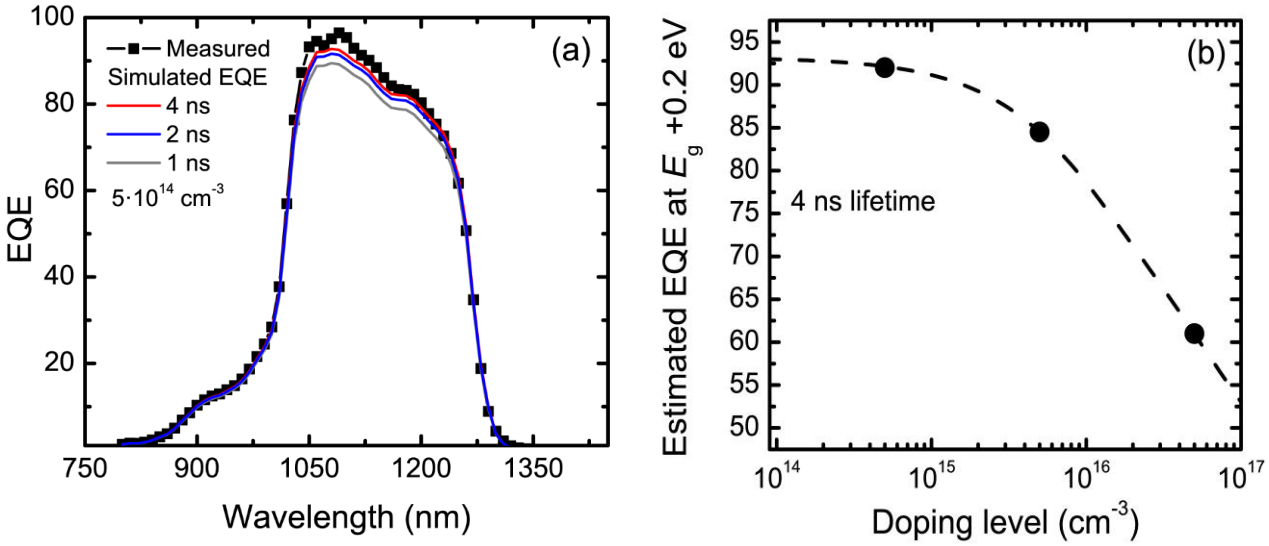

Figure 4. (a) *PC1D modelled EQE curves of the bottom cell with lifetimes of 1 ns to 4 ns and the experimental EQE measurement. (b) Estimated EQE values for different background doping levels for the bottom cell with photon energy of E_g + 0.2 eV and carrier lifetime of 4 ns.*

The bottom cell suffers slightly from transmission and collection losses due to unideal charge carrier collection efficiency. We estimate that for the bottom cell we have 1 μm wide depletion region and between 1.5 μm and 2.1 μm long diffusion length. The estimation is based on the fitting of the PC1D modelled EQE data to the actual EQE performance of the bottom cell. Details for PC1D modelling of single junction dilute nitride cells are reported elsewhere [23]. Extremely good correlation between the measured and PC1D simulated EQE curves was obtained with $5 \cdot 10^{14}$ cm^{-3} background doping level and with 2–4 ns lifetimes (see Figure 4a). The EQE values strongly depend on the background doping level, which can be seen from Figure 4b. For the studied 4J cell, extremely low background doping levels are needed to achieve high efficiencies. To increase the collection efficiency of bottom cell, even thicker bottom junction and improved charge carrier lifetimes would be needed.

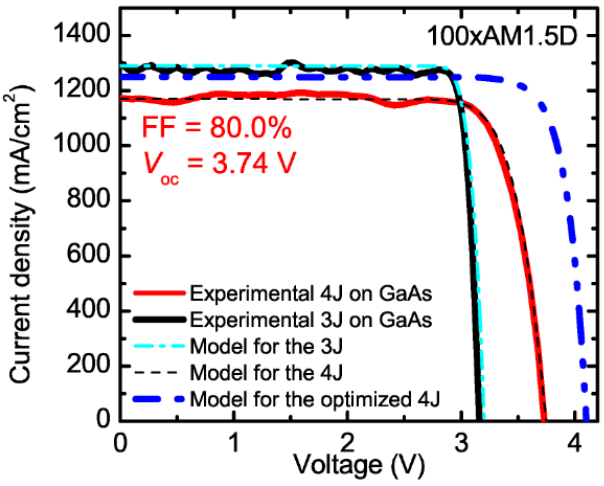

Figure 5. *I-V characteristics of 3J and 4J cells grown by MBE and measured at 100x and 25°C, and modelled cell performances at 100x. Estimated IV-characteristics for the optimized 4J are also included for comparison.*

CPV performance measured at 100x is presented in Figure 5. The cell efficiency with the given grid design peaks at 100-200 suns illumination. We estimate the cell maximum efficiency under concentrated light to be 36.5±2%. Theoretically, the cell could reach an efficiency of 43% at the given conditions (see Figure 2c), from which 81% to 88% is achieved. Based on the separate measurements, the top cell pair exhibit a V_{oc} of 2.6 V at 100 suns and the bottom pair V_{oc} is 1.2 V, which totals 3.8 V, as seen in the measurement presented in Figure 5. Figure 5 also compares the 4J cell with the GaInP/GaAs/GaInNAsSb 3J cell, modelled IV-curves for the experimental cells, and projected IV-curve for the optimized 4J. We see that the 4J cell exhibits 0.6 V higher V_{oc}, which shows that the cell has a practical potential to reach high efficiencies. We estimate that the high concentration efficiency of the 4J is currently limited by the lateral current spreading of the charge carriers in the thin top junction, which can be also seen in the data as an increase of the series resistance.

We are currently working on designs that should provide significantly improved current spreading for the cell to achieve the performances simulated in this work. As the structure optimization is at an early stage, voltage is also lost due to non-optimal interfaces between the new junctions. We also continuously develop ARC designs that would enable better collection efficiencies for the top and bottom cells. In addition, the development of a more transparent top tunnel junction would provide additional efficiency boost for the cell.

5. Conclusions

We have studied monolithic 4J solar cells fabricated on GaAs substrates using simulations and experiments. The solar cell incorporates junctions with 1.9 eV, 1.4 eV, 1.2 eV and 0.90 eV bandgaps. An important aspect revealed by the simulation is that it would be beneficial to use a 0.90 eV bottom cell instead of a 0.95 eV bottom cell. The simulations reveal that the cell can exhibit 34.7% and 32.4% efficiencies at one sun with AM1.5D and AM0 spectrum, respectively. Correspondingly, for 1000 suns AM1.5D illumination, the simulated efficiency reaches as value of 46.4%. For the calculations we assumed an average EQE of 95% and that the dilute nitride cells exhibit a one sun bandgap-voltage offset of 0.5 V. An experimental solar cell was grown by MBE. The cell exhibited promising characteristics, with up to 91% of simulated average EQE and up to 87% of the simulated one sun V_{oc}. Under 100 suns intensity, the experimental cell exhibited up to 36.5±2% efficiency. For the understanding of the GaInNAsSb bottom junction material characteristics, we also performed comparative study between the PC1D simulated EQE values and the measured bottom cell EQE. Based on the best fits, we estimate that the used GaInNAsSb bottom junction material exhibit a background doping level of $5 \cdot 10^{14}$ cm^{-3} and up to 2–4 ns minority charge carrier lifetime. For the improved current generation of the bottom cell, extremely low doping levels ($<<10^{15}$ cm^{-3}) and high minority carrier lifetimes (>>4 ns) should be achieved. Moreover, to fulfill its theoretical potential, the cell should employ improved ARCs and tunnel junctions, which are subject of current developments.

Acknowledgements

We would like to acknowledge the European Research Council (ERC AdG AMETIST, #695116) for financial support. Dr. Ville-Markus Korpijärvi, Dr. Jukka Viheriälä, Mervi Koskinen and Antti Aho are acknowledged for developing the 1.2 μm laser diode used for the QE measurements of the 4J cell.

References

[1] C.H. Henry, Limiting efficiencies of ideal single and multiple energy gap terrestrial solar cells, Journal of Applied Physics, Vol. 51, No. 8, 1980, pp. 4494-4500.

[2] F. Dimroth, M. Grave, P. Beutel, U. Fiedeler, C. Karcher, T.N.D. Tibbits, E. Oliva, G. Siefer, M. Schachtner, A. Wekkeli, A.W. Bett, R. Krause, M. Piccin, N. Blanc, C. Drazek, E. Guiot, B. Ghyselen, T. Salvetat, A. Tauzin,

T. Signamarcheix, A. Dobrich, T. Hannappel, K. Schwarzburg, Wafer bonded four-junction GaInP/GaAs//GaInAsP/GaInAs concentrator solar cells with 44.7% efficiency, Progress in Photovoltaics: Research and Applications, Vol. 22, No. 3, 2014, pp. 277-282.

[3] R. M. France, J. F. Geisz, I. García, M. A. Steiner, W. E. McMahon, D. J. Friedman, T. E. Moriarty, C. Osterwald, J. S. Ward, A. Duda, M. Young, W. J. Olavarria, Design Flexibility of Ultrahigh Efficiency Four-Junction Inverted Metamorphic Solar Cells, IEEE Journal of Photovoltaics, Vol. 6, No. 2, 2016, pp. 578-583.

[4] M.A. Green, Y. Hishikawa, W. Warta, E.D. Dunlop, D.H. Levi, J. Hohl-Ebinger, A.W.H. Ho-Baillie, Solar cell efficiency tables (version 50), Progress in Photovoltaics: Research and Applications, Vol. 25, No. 7, 2017, pp. 668-676.

[5] M.A. Green, K. Emery, Y. Hishikawa, W. Warta, E.D. Dunlop, Solar cell efficiency tables (version 41), Progress in Photovoltaics: Research and Applications, Vol. 21, No. 1, 2013, pp. 1-11.

[6] A. Aho, R. Isoaho, A. Tukiainen, G. Gori, R. Campesato, M. Guina, Dilute nitride triple junction solar cells for space applications: Progress towards highest AM0 efficiency, Progress in Photovoltaics: Research and Applications, Vol. 1-5, 2018.

[7] R. King, P. Colter, D. Joslin, K. Edmondson, D. Krut, N. Karam, S. Kurtz, High-voltage, low-current GaInP/GaInP/GaAs/GaInNAs/Ge solar cells, Photovoltaic Specialists Conference, 2002. Conference Record of the Twenty-Ninth IEEE, IEEE, pp. 852-855.

[8] S. Essig, E. Stammler, S. Ronsch, E. Oliva, M. Schachtner, G. Siefer, A. Bett, F. Dimroth, Dilute nitrides for 4-and 6-junction space solar cells, Proceedings of the 9th European Space Power Conference, ESA SP, Vol. 690, 2011.

[9] M. Ochoa, I. García, I. Lombardero, L. Ayllón, I. Rey-Stolle, C. Algora, A. Johnson, J.I. Davies, K.H. Tan, W.K. Loke, S. Wicaksono, S.F. Yoon, E. Ochoa-Martínez, M. Gabás, Modelling of lattice matched dilute nitride 4-junction concentrator solar cells on Ge substrates, AIP Conference Proceedings, Vol. 1766, No. 1, 2016, pp. 080003.

[10] G. Bauhuis, P. Mulder, E. Haverkamp, J. Huijben, J. Schermer, 26.1% thin-film GaAs solar cell using epitaxial lift-off, Solar Energy Materials and Solar Cells, Vol. 93, No. 9, 2009, pp. 1488-1491.

[11] A. van Geelen, P.R. Hageman, G.J. Bauhuis, P.C. van Rijsingen, P. Schmidt, L.J. Giling, Epitaxial lift-off GaAs solar cell from a reusable GaAs substrate, Materials Science and Engineering: B, Vol. 45, No. 1–3, 1997, pp. 162-171.

[12] R. H. Horng, M. C. Tseng, F. L. Wu, C. H. Li, C. H. Wu, M. D. Yang, Thin Film Solar Cells Fabricated Using Cross-Shaped Pattern Epilayer Lift-Off Technology for Substrate Recycling Applications, IEEE Transactions on Electron Devices, Vol. 59, No. 3, 2012, pp. 666-672.

[13] A. Aho, A. Tukiainen, V. Polojärvi, M. Guina, Performance assessment of multijunction solar cells incorporating GaInNAsSb, Nanoscale research letters, Vol. 9, No. 1, 2014, pp. 1-7.

[14] R.R. King, D. Bhusari, A. Boca, D. Larrabee, X.-. Liu, W. Hong, C.M. Fetzer, D.C. Law, N.H. Karam, Band gap-voltage offset and energy production in next-generation multijunction solar cells, Progress in Photovoltaics: Research and Applications, Vol. 19, No. 7, 2011, pp. 797-812.

[15] A. Kirk, High efficacy thinned four-junction solar cell, Semiconductor Science and Technology, Vol. 26, No. 12, 2011, pp. 125013.

[16] A. Aho, A. Tukiainen, V. Korpijärvi, V. Polojärvi, J. Salmi, M. Guina, Comparison of GaInNAs and GaInNAsSb solar cells grown by plasma-assisted molecular beam epitaxy, 8TH INTERNATIONAL CONFERENCE ON CONCENTRATING PHOTOVOLTAIC SYSTEMS: CPV-8, AIP Publishing, pp. 49-52.

[17] A. Aho, V. Korpijärvi, A. Tukiainen, J. Puustinen, M. Guina, Incorporation model of N into GaInNAs alloys grown by radio-frequency plasma-assisted molecular beam epitaxy, Journal of Applied Physics, Vol. 116, No. 21, 2014, pp. 213101.

[18] A. Aho, V. Polojärvi, V. Korpijärvi, J. Salmi, A. Tukiainen, P. Laukkanen, M. Guina, Composition dependent growth dynamics in molecular beam epitaxy of GaInNAs solar cells, Solar Energy Materials and Solar Cells, Vol. 124, 2014, pp. 150-158.

[19] A. Aho, R. Isoaho, A. Tukiainen, V. Polojärvi, T. Aho, M. Raappana, M. Guina, Temperature coefficients for GaInP/GaAs/GaInNAsSb solar cells, 11TH INTERNATIONAL CONFERENCE ON CONCENTRATOR PHOTOVOLTAIC SYSTEMS: CPV-11, AIP Publishing, pp. 050001.

[20] V. Korpijärvi, J. Viheriälä, M. Koskinen, A.T. Aho, M. Guina, High-power temperature-stable GaInNAs distributed Bragg reflector laser emitting at 1180 nm, Opt.Lett., Vol. 41, No. 4, 2016, pp. 657-660.

[21] P. Espinet-González, I. Rey-Stolle, M. Ochoa, C. Algora, I. García, E. Barrigón, Analysis of perimeter recombination in the subcells of GaInP/GaAs/Ge triple-junction solar cells, Progress in Photovoltaics: Research and Applications, Vol. 23, No. 7, 2015, pp. 874-882.

[22] J. F. Geisz, M. A. Steiner, N. Jain, K. L. Schulte, R. M. France, W. E. McMahon, E. E. Perl, D. J. Friedman, Building a Six-Junction Inverted Metamorphic Concentrator Solar Cell, IEEE Journal of Photovoltaics, Vol. PP, No. 99, 2017, pp. 1-7.

[23] A. Tukiainen, A. Aho, V. Polojärvi, R. Ahorinta, M. Guina, High Efficiency Dilute Nitride Solar Cells: Simulations Meet Experiments, Journal of Green Engineering, Vol. 5, No. 3, 2015, pp. 113-132.